Hydrol. Earth Syst. Sci. Discuss., doi:10.5194/hess-2016-662, 2017
Manuscript under review for journal Hydrol. Earth Syst. Sci.
Published: 9 January 2017

Hydrology and Earth System Sciences
Open Access
EGU
Discussions

Effectiveness of distributed temperature measurements for early detection of piping in river embankments

Silvia Bersan[1], André R. Koelewijn[2], Paolo Simonini[1]

[1] Department of Civil, Environmental and Architectural Engineering, University of Padova, Padova, 35131, Italy
[2] Department of Dike Technology, Deltares, Delft, 2600 MH, the Netherlands.

Correspondence to: Silvia Bersan (silvia.bersan@dicea.unipd.it)

Abstract. Internal erosion is the cause of a significant percentage of failure and incidents involving both dams and river embankments in many countries. In the past 20 years the use of fibre-optic Distributed Temperature Sensing (DTS) in dams has proved to be an effective tool for detection of leakages and internal erosion. This work investigates the effectiveness of DTS for dike monitoring, focusing on early detection of backward erosion piping, a mechanism that affects the foundation layer of structures resting on permeable, sandy soils. The paper presents data from a piping test performed on a large-scale experimental dike equipped with a DTS system together with a large number of accompanying sensors. The effect of seepage and piping on the temperature field is analysed, eventually identifying the processes that cause the onset of thermal anomalies around piping channels and thus enable their early detection. Making use of dimensional analysis, the factors that influence that thermal response of a dike foundation are identified. Eventually some tools are provided that can be helpful for the design of monitoring systems and for interpretation of temperature data.

Keywords: Distribute Temperature Sensing, fibre optics, internal erosion, piping, levee monitoring

Hydrol. Earth Syst. Sci. Discuss., doi:10.5194/hess-2016-662, 2017
Manuscript under review for journal Hydrol. Earth Syst. Sci.
Published: 9 January 2017

Hydrology and Earth System Sciences
Discussions

1 Introduction

The word piping is often generically used in the literature to indicate different kinds of internal erosion, generating confusion and inaccuracy. In this paper the word *piping* refers to the development of erosion channels or 'pipes' in a sandy soil laying underneath a water retaining structure with an impervious (clayey or concrete) base (Figure 1). The International Commission On Large Dams has defined this mechanism *backward erosion piping* (ICOLD, 2015).

The erosion process typically starts at the downstream side of the structure, where the flow lines converge and an unfiltered exit for the flow is present. The pipes then grow backwards and when one of them reaches the upstream side a pressure surge can cause its excessive enlargement often followed by the failure of the embankment.

Backward erosion piping represents a significant problem for the safety of river and sea dikes located in delta areas, including, e.g., the Po plain in Italy and large part of the Netherlands.

A number of studies describing the process and suggesting failure criteria have been conducted. The first studies date back to the beginning of the last century (Clibborn and Beresford, 1902; Bligh, 1910; Terzaghi, 1922) and are still at the base of the rules included in national codes (TAW, 1999; USACE, 2005). Many other experimental and theoretical studies followed across the years (e.g. WES, 1956; De Wit et al., 1981; Weijers and Sellmeijer, 1993; Muller-Kirchenbauer et al., 1993; Schmertmann, 2000; Ojha and Singh, 2003; Sellmeijer et al., 2011; Van Beek et al., 2011). Later studies show that researchers are still investigating the subject to improve the theoretical model (e.g. Richards and Reddy, 2014; Van Beek et al., 2014a,b; Allan et al., 2014) and find cost-effective countermeasures (Koelewijn et al., 2014; Wang et al., 2015).

The uncertainty due to spatial variability in the subsoil composition adds up to the uncertainty associated with the theoretical model. Usually only point measurements and cross-section calculations are available, while large uncertainties in the longitudinal direction are present because of both the extent of the areas to be assessed and the likelihood that ancient riverbeds and crevasse channels cross the actual course of the river causing a local change in the type of sediments. In Kanning (2012) the probability of failure by piping is calculated including the uncertainties associated with the fluctuation of soil properties in space.

When the uncertainty is high, monitoring systems can come in handy, since they help understanding and quantifying the ongoing processes as well as to identifying weak spots where failure is more likely to occur. The latter generally coincides with zones where stronger seepage is recorded. Identification of the most hazardous stretches along a dike facilitates a rational allocation of the resources for both inspection activities and improvement works.

Monitoring systems can also work as early warning tools. In this case their effectiveness depends on how much in advance they can detect the incipit of failure in comparison with the time necessary to undertake and complete the actions aimed at preventing the collapse or to prepare for evacuation of the surrounding areas.

In river embankments, a few sudden failures promoted by piping have been observed (e.g. Imre et al., 2015) but in most cases the erosion process is slow enough to allow an effective intervention, which consists in building temporary sandbag

Hydrol. Earth Syst. Sci. Discuss., doi:10.5194/hess-2016-662, 2017
Manuscript under review for journal Hydrol. Earth Syst. Sci.
Published: 9 January 2017

rings around the sand-boils to stop or slow down the sand transport. The double possibility, of either fast or slow evolution of the mechanism, finds confirmation in theory (Van Beek et al., 2014a) and experiments (Koelewijn and Taccari, 2016).

Identification of piping is generally performed through visual inspections during flood periods. However, this is often difficult because of the lack of personnel and because sand-boils can be difficult to spot: these can be hidden by vegetation or by ponding water at the embankment toe, can develop in ditches or hundreds of meters away from the dike toe. In this context sensors represent "extra eyes" with the capability of extending the control domain beyond the visible and anticipating the detection of anomalies (Peeters et al., 2013).

The use of DTS for early detection of internal erosion is nowadays common practice in dam monitoring. However specific studies are required to apply the same technique to river embankments, since there are some differences between dams and river embankments which can affect the heat transfer processes, the most important being the size of the embankment and the duration of the hydraulic loads.

This paper illustrates the response of a distributed temperature sensor installed in a test dike in which piping was induced by gradually increasing the hydraulic load over a 5-day period. The effects of seepage and piping on the temperature distribution under a dike are analysed and some indications are provided for predicting the effectiveness of the thermometric method on a case by case basis.

2 Early detection of internal erosion

Internal erosion is hard to identify using conventional geotechnical instrumentation, because its effect on porewater pressures is highly localised. Both theoretical considerations (Ng & Oswalt, 2010) and field data from the test described here (Bersan, 2015) show that the draining effect of a pipe affects a region surrounding the pipe having a radius in the order of 1 m. Consequently, a monitoring system relying on measurements of porewater pressure would require a high, and therefore uneconomical, number of sensors, even for controlling short stretches.

In the last decades, many efforts have been made to identify new parameters linked to seepage and internal erosion which are measurable by means of extensive technologies. Among these are electrical resistivity, self-potential and temperature (Sheffer et al., 2009). These methods have a common feature: they provide spatially distributed measurements. Unfortunately they also have a common shortcoming: they measure quantities that are influenced by a large number of variables besides the occurrence of internal erosion, which makes data interpretation not straightforward and ambiguous.

The thermometric method is based on the principle that heat transfer in soils mostly occurs by conduction, but when the pore water flows at significant velocity, then the transfer of heat promoted by the fluid flow, also denominated advection, becomes predominant.

Because of conduction, the temperature in the soil at less than 10-15 m of depth fluctuates annually in response to the variations of the air temperature and solar radiation. Below this zone the temperature mildly increases with depth with a gradient that in the upper part of the Earth's crust is 25 °C/km on average.

Hydrol. Earth Syst. Sci. Discuss., doi:10.5194/hess-2016-662, 2017
Manuscript under review for journal Hydrol. Earth Syst. Sci.
Published: 9 January 2017

While moderate seepage flow occurring in the soil does not affect the temperature field determined by heat conduction, significant seepage (rates higher than 10^{-7} - 10^{-6} m/s) produce variations in the soil temperature. Since internal erosion promotes the formation of zones of higher permeability and, consequently, a local increase of seepage rate, it is expected that it also causes a local variation of the temperature field. Johansson and Sjödal (2009) observed that, in dams, the regions affected by internal erosion are typically characterized by a temperature similar to the reservoir water, while the temperature in the other regions of the flow domain is nearly unaffected by the reservoir temperature.

In the past, temperature measurements were performed in embankment dams using thermocouples installed at different depths inside standpipes. After fibre-optic Distributed Temperature Sensing (DTS) systems became available on the market, continuous measurements over kilometres became possible with a spatial resolution down to 1 m. Optical cables can now be easily installed also in existing embankments, buried in the soil lengthwise the dike, in a narrow trench excavated at the toe or under the surface of the downstream slope. Details on the functioning principles of fibre-optic sensors are given in Henault et al. (2010).

There are two variations of the DTS technique. The active method, or heat pulse method, consists in heating the cable containing the optical fibres and observing how it cools down: higher seepage flows correspond to a faster cooling. The passive method, i.e. the method adopted in the test described in this paper, consists in measuring the temperature variations naturally induced in the soil by seepage.

In the past two decades the thermometric method has gained increasing acceptance (Johansson & Sjödahl, 2009) and common applications to date include detection of leakage from tailing dams, waterproofed basins, at the joints of concrete-face rock-fill (CFRF) dams and canal dikes.

Very few installations concern river or sea dikes. However, the diffusion of DTS systems has promoted a significant decrease of their costs in the past decade and a further reduction is expected in the coming years, making the technique appealing also for applications where the economic interests at stake are smaller, as in river management.

3 Trial test of a dike subject to piping

In September 2012, in Booneschans, in the Northeast of the Netherlands, backward erosion piping was induced in two test embankments. The experiments were part of the IJkdijk (Dutch term for calibration dike) program, a research program initiated in 2005 with the double goal of testing new monitoring techniques under field conditions and advancing the knowledge on geotechnical failure mechanisms at the large scale. The project involved research institutes, sensors manufacturers and water authorities. This paper describes the test conducted on the “west dike”, which is located on the right in Fig. 2.

Hydrol. Earth Syst. Sci. Discuss., doi:10.5194/hess-2016-662, 2017
Manuscript under review for journal Hydrol. Earth Syst. Sci.
Published: 9 January 2017

3.1 Set up

The trial dike was surrounded by a containing ring forming a reservoir with a volume of about 2000 m^3. A lower and smaller dike ring enclosed a second basin used to control the downstream water level and ensure full saturation of the foundation layer after careful preparation applying 50% vacuum during saturation. The dike was 3.5 m high, 19 m long and 15 m wide at the bottom.

The geometry of the dike is depicted in Fig. 3. The foundation consisted of a sand layer with a thickness of 3.25 m (3.00 m by design). An impermeable foil separated this layer from the in situ soil. The foundation soil was a uniform sand characterized by an average grain size of d_{50} = 0.30 mm and a uniformity coefficient $U=d_{60}/d_{10}$= 1.69. The lower part of the dike was made of a 0.7 m well-compacted clay layer. Given its low permeability, the clay layer separated the hydraulic fluxes occurring in the foundation from the fluxes affecting the embankment. The dike body was made formed by a 1.7 m high, poorly-compacted small clay dike at the upstream side and a sand core covered by organic clay. This composition is representative of a number of small dikes around the Netherlands.

The field trial was named All-In-One Sensor Validation Test, since the occurrence of more than one failure mechanism was possible. By design, the failure of the dike described in this paper could occur either because of piping through the foundation soil or because of micro-instability of the sand core. Failure by overtopping of the crest with subsequent erosion of the downstream slope was also a possibility, in case the previous two did not occur earlier.

Throughout the test, the dike was monitored using a number of innovative technologies with the aim of testing the capability of such technologies in predicting imminent failure in field conditions. The technologies included distributed fibre-optic strain and temperature sensing, fibre Bragg grating (FBG), ground-based radar, infrared thermography, ground penetrating radar and electrical resistivity.

The distributed fibre-optic sensor consisted of 2 single-mode and 2 multi-mode fibres encased in a geotextile strip (Fig. 4). A single strip was arranged in 8 profiles in the length of the dike: five at the interface between the sand layer and the bottom of the dike (labelled F1 to F5 in Fig. 3), three on the downstream slope of the dike (labelled F6 to F8). Single-mode fibres were connected to a reading unit exploiting stimulated Brillouin scattering to measure strain while multi-mode fibres were connected to a reading unit exploiting Raman scattering to measure temperature. Temperature changes were measured with an accuracy of 0.1 °C, a spatial resolution of 1 m along the sensor and a frequency of two measurements per hour. In addition, an infrared camera mapped the surface temperature of the downstream slope (and of part of the upstream and downstream basins).

The dike was also equipped with conventional pore pressure transducers, which provided reference measurements and allowed to closely monitor the growth of the pipes: 4 lines (labelled P1 to P4 in Fig. 3) consisting of 17 sensors each had been installed at the top of the foundation soil during construction and 3 lines (labelled P5 to P7) consisting of 3 sensors each had been installed in the sand core, right above the clay layer. The conventional monitoring also included two liquid level

Hydrol. Earth Syst. Sci. Discuss., doi:10.5194/hess-2016-662, 2017
Manuscript under review for journal Hydrol. Earth Syst. Sci.
Published: 9 January 2017

sensors to record the water level in the upstream and downstream reservoirs, a flow meter placed at the discharge point of the downstream basin, visual inspection and hand readings of discharge and basin levels performed at regular intervals.

3.2 Execution

The dike was forced to collapse slowly, in a controlled manner, in order to provide the largest amount of data possible to aid in evaluating the performance of the sensors and understanding the ongoing mechanisms. The water level was increased in steps in the upstream basin, while the downstream basin was maintained at an almost constant level of about 10 cm above the surface of the sand layer to ensure full saturation. The resulting load is displayed in Fig. 5.

The bulk hydraulic conductivity of the sand layer, as calculated from flow measurements performed at the discharge point of the downstream basin before piping occurred, was $K = 1.5 \cdot 10^{-4}$ m/s.

The first sand-boil was detected at location x = 5.2 m after two days of testing (t = 45 h). Two among the pore pressure sensors of line P1 (x = 4.8 and x = 5.8 m) showed a small pressure drop two hours before the sand-boil was detected. The first sand-boil developed at a hydraulic load of 1.5 m, which corresponds to a percolation factor of 10. The percolation factor, as defined in Bligh (1910), is the ratio between seepage length L and hydraulic load H (Fig. 1). It represents the simplest way of expressing the susceptibility of a structure to backward erosion. A structure is considered unsafe when L/H < 15 for fine sands and L/H < 12 for coarse sands.

Soon after the load was increased to 1.75 m at t = 50 h, three other pore pressure sensors in line P1 showed a small drop, which was later confirmed by the discovery of three new sand-boils at x = 8.7, 11.2 and 11.7 m.

At t = 55 h, after the load was further increased by 10 cm, pressure drops occurred in line P2, indicating that piping channels grew and reached that far. From that moment on, sand transport occurred continuously, as revealed by the size of the sand-boils increasing with time. Two more sand-boils were detected, at x = 17.4 m and x = 7.0 m, respectively at t = 60 h and at t = 65 h. Erosion stopped after the opening of a controllable drainage tube that had been installed in the dike foundation as a countermeasure (its position is indicated in Fig. 3).

The tube was eventually closed to bring the dike to collapse. However, the dike did not fail because of piping. Since no significant pore pressure drop was recorded during the test by the transducers at line P3, it can be assumed that no pipe grew that far and thus no pipe reached the upstream side. The dike failed because of instability of the downstream slope developed on the 5th day of testing, after the saturation line in the sand core reached the downstream toe causing an excessive strength reduction.

From the data collected during the field trial the size of the pipes can be roughly inferred. The length of the pipes in the first stages can be deduced knowing that the pipes had reached line P1 of pore pressure transducers, but not yet line P2. From the size of the sand-boils recorded during the visual inspections the volume of sand eroded is calculated and from these data the cross-sectional area of a pipe (or a multitude of pipes that developed behind a sand-boil) results to be between 2.5 and 5 cm^2.

Hydrol. Earth Syst. Sci. Discuss., doi:10.5194/hess-2016-662, 2017
Manuscript under review for journal Hydrol. Earth Syst. Sci.
Published: 9 January 2017

3.3 Temperature data

Temperature measurements started 7 days before the beginning of the test. Fig. 6 shows the evolution of the temperature measured at lines F1 to F5 at the middle section of the dike (x =10 m).

From the beginning of the measurements (t = 0) to the beginning of the test (t = 7 days), the temperature at the bottom of the dike was nearly constant. Minor differences, smaller than 1 °C, were due to different distances of the measuring lines from the surface and different expositions (south or north) of the slope under which the point is located. The only exception is represented by line F1. Being the shallowest and lying under the slope facing south, line F1 was the most influenced by the variations occurring in the external environment. The temperature nearly monotonically increased until the beginning of the test, a likely consequence of the increase in the average daily temperature and solar radiation during the week preceding the test.

Few hours after the beginning of the test, the temperature recorded at F5 started increasing, suggesting that the reservoir water was warmer than the foundation bulk. Unfortunately, measurements of the water temperature in the upstream basin were not available due to technical problems. At lines F4 and F3 the warm front arrived after 2 and 3 days respectively. On the contrary, at F2 the temperature started to slowly decrease soon after the beginning of the test and kept decreasing until the arrival of the warm front, more than 3 days later. At line F1 the temperature decreased significantly during the test and the warm front never arrived.

The spectrogram in Fig. 7 depicts the temperature measured at the most downstream position F1. Starting from 55 h, localized temperature drops are visible at the locations where piping was observed, approximately at x = 5, 11 and 17 m. The time coincides with the recording of the first pressure drops at line P2. No anomaly in the temperature is detected at 43 h, when the first pressure drops where recorded by the downstream line P1. This is consistent with the position of F1, which is located between P1 and P2. The local temperature variations measured during the test were all smaller than 1 °C.

Since the temperature of the reservoir water was higher than the initial temperature of the dike, it was expected that piping produced a localized temperature increase at the piping locations rather than a decrease. The unexpected temperature drops are however clarified by looking at the contours in Fig. 8, which shows a plan view of the temperature at the bottom of the dike at four successive times. As expected, the inflow water preserved its initial temperature, promoting the advance of a warm thermal front. At the same time, however, the inflow water pushed downstream the water initially present under the dike crest, promoting the advance of a cold thermal front towards the (initially) warmer downstream toe. The cold front advanced faster at the piping locations than in the portion unaffected by piping, thus producing the measured localized temperature drops. A temperature increase at the piping locations would have occurred only if the pipes had progressed backwards sufficiently to reach the approaching warm thermal front. This likely happened towards the end of the test.

In the 100 h contour plot, preferential flow paths can be observed at the sides. Here warm water flows faster than in the centre of the dike. As no sand-boil was observed at the sides, these preferential paths are believed to be a consequence of the discontinuity between the soil and the impermeable foil delimiting the artificial basin. These minor leakages could not be

Hydrol. Earth Syst. Sci. Discuss., doi:10.5194/hess-2016-662, 2017
Manuscript under review for journal Hydrol. Earth Syst. Sci.
Published: 9 January 2017

Hydrology and Earth System Sciences
Discussions

identified by the pore pressure readings. The contours also show that the temperature is not uniform along the x-axis (except downstream), neither in absence of flow ($t \leq 0$) nor with seepage occurring ($t > 0$). The temperature is indeed higher at the centre than at the borders. This can be ascribed to the 3-d character of the test facility, in opposition to a real dike where the longitudinal dimension is much larger than the transversal dimension.

As suggested by Khan (2008), temperature gradients in the longitudinal direction can be very informative for anomaly detection. Fig. 9 shows the gradients along the fibre F1, calculated as the temperature difference between two points along the fibre located 1 m apart. At locations x = 5 m and x = 11 m, where sand-boils have been observed, the gradients start to increase at 50 h, stabilize around a value of 0.3 between about 65 and 85 h , when the hydraulic load is kept nearly constant and then decrease after 85 h, when the hydraulic load is increased at a rate of roughly 12 cm per hour. At x = 18 m, where a sand-boil was observed starting from 60 h, the large magnitude of the spatial temperature gradient is likely to derive from the superposition of two effects: the temperature decrease caused by piping at that location and the temperature increase caused by the leakage along the foil at x = 19 m (cf. Fig. 8). For comparison, the graph also reports the gradients at x = 14 m where no sand-boil was observed, at least not until 90 h, when visual inspection was stopped for safety reasons.

Fig. 10 shows the temperature gradient in the seepage direction, calculated in proximity of the downstream toe, between fibre F1 and F2, at two locations: x = 11 m, where piping occurred, and x = 14, where no trace of piping was detected. The gradient is non-zero at the beginning of the test and keeps decreasing during the test as a consequence of the seepage flow. After 50 h the gradient decreases faster at the location affected by piping. Here, after 90 h the gradient turns negative, suggesting that the warm thermal front coming from upstream is approaching the head of the pipe.

4 Interpretation of temperature data from the field trial

During the experiment the seepage flow caused significant variations of the temperature in the entire dike foundation. This was likely due to the seepage velocity being high enough to influence the soil temperature – in more technical language, advective fluxes were prevailing - not only in the zones affected by internal erosion but also in the surrounding soil. For this reason, the mechanism that promoted the formation of piping-induced thermal anomalies was not, as commonly found in the literature, the prevalence of advection in the eroded regions in opposition to the purely conductive behavior of the regions unaffected by piping. This occurs because the assumption of conductive behavior in the unaffected regions (Johansson and Hellström 2001; Johansson and Sjödal 2009) only applies to low permeability bodies such as dam cores.

The evolution of the temperature under the test dike was simulated using COMSOL Multiphysics®, a finite element code that allows coupling of seepage and heat transfer. Details on the numerical model are available in Bersan (2015). The numerical model, after being validated with the field data, was also used to predict the behavior of the test dike over a period longer than the test duration. In the simulation, inflow temperature and hydraulic load were assumed to be constant over time and equal to 16 °C and 3 m respectively. The latter corresponds to an average seepage velocity of $3 \cdot 10^{-5}$ m/s. The advance of the thermal front as obtained from the simulation is depicted in Fig. 11. It is clear that after some time the temperature

Hydrol. Earth Syst. Sci. Discuss., doi:10.5194/hess-2016-662, 2017
Manuscript under review for journal Hydrol. Earth Syst. Sci.
Published: 9 January 2017

under the dike is nearly everywhere equal to the reservoir temperature. However, it takes more than four days, that was the duration of the test, for the thermal front to reach the downstream toe. This means that in a small dike with a permeable foundation an advective front can propagate over the whole seepage length but this requires some time. Differently from dams, many levees are subject to significant hydraulic loads for very short periods, in the order of half a day to few days. The time required for the thermal front to reach the downstream toe can therefore be of the same order or larger than the duration of typical flood events.

In the test the passive thermometric method (Sec. 2) was adopted, which is also called gradient method, because it is believed that a necessary condition for its effectiveness is the existence of a temperature gradient between the waterbody and the soil. It is clear that during the test the temperature of the waterbody did not have any influence on the formation of the thermal anomalies, as otherwise a local temperature increase rather than a decrease would have been observed in the pipes. The data suggest that a sufficient condition for the formation of a thermal anomaly is the existence of a thermal gradient along the pipe, so that the temperature of the water entering in the pipe – mostly close to the *head* (Fig. 1) – is different from the temperature of the soil at the location where the sensor is placed, generally at the downstream toe of the dike and thus very close to the *tail* of the pipe. The test results suggested that there are at least two possible mechanisms that can produce a temperature gradient along a pipe.

The first mechanism requires that two conditions are satisfied: (i) a temperature gradient exists between the waterbody and the soil region where the sensor is placed, (ii) the characteristics of the problem (geometry, soil properties, hydraulic load) are such that a thermal front propagates from the upstream side up to the head of the pipe during the flood event. When a pipe extends for the whole seepage length - or nearly - condition (i) becomes a sufficient condition for the development of a gradient along a pipe. However, when dealing with backward erosion piping, a pipe extending over a large part of the seepage path is symptom of a situation already close to the collapse. On the contrary, an effective monitoring must be able to detect pipes in their early stage of development. Condition (ii) can thus be reformulated as follows if early detection is the goal: the characteristics of the system must be such that a thermal front propagates from upstream up to the downstream toe during a flood event.

There second mechanisms relies on the existence of a temperature gradient at the base of the dike – and consequently along a pipe – before seepage occurs. This will be named here *initial gradient* and is due to the interaction between the soil and the atmosphere. In low permeability soils, where conduction prevails, the effect exerted by the seepage flow is to alter the initial gradient only in the pipes. In more permeable materials the initial gradient is altered everywhere by seepage, but in the pipes it is modified more quickly than in the unaffected regions.

It is interesting to note that the temperature gradients along the dike toe (Fig. 9) decrease towards the end of the test although it is unlikely that the preferential flow paths influencing them had stopped. A reasonable explanation is that the initial temperature gradient at the toe was completely hindered by the seepage flow so that the gradient tends to zero along the pipes and the conditions required for the formation of thermal anomalies were not satisfied anymore. This suggests that the alteration of an initial gradient (mechanism 2) is exploitable for detection at the beginning of a flood event but tends to

Hydrol. Earth Syst. Sci. Discuss., doi:10.5194/hess-2016-662, 2017
Manuscript under review for journal Hydrol. Earth Syst. Sci.
Published: 9 January 2017

Hydrology and Earth System Sciences
Discussions

diminish its information content after some time. On the contrary, the advancement of the upstream thermal front up to the pipe head (mechanism 1) may require some time from the beginning of the flow. The gradients in the seepage direction, as depicted in Fig. 10, suggest that the thermal front reached the head of the pipe close to the end of the test. The two mechanisms can therefore act in synergy, one after the other, allowing continuous detection of piping. The data also suggest that a decrease of the magnitude of a thermal anomaly cannot be automatically interpreted as a decrease of the magnitude of the leakage and that for dikes subject to transient hydraulic loads it is not possible to define a unique relationship between thermal anomalies and leakage magnitude, as it was attempted for channel dikes (Artiéres et al., 2007).

The temperature anomalies detected were of very small extent, in the order of few decimals of a degree. Since the spatial resolution of the sensor is much larger than the width of a single pipe, it was initially feared that the averaging performed by the sensor was reducing the actually detected magnitude of the temperature anomalies. However, when the pipes developed, the temperature difference between F1 and F2, which was responsible for the anomalies produced by piping, was less than 1 °C and thus the small extent of the anomalies was in large part to be ascribed to the measurand rather than to the measuring system. The possibility that a branched net of very small pipes formed rather than a single larger channel, as observed in medium-scale experiments (Weijers and Sellmeijer, 1993) and supported by the comparison of field pore pressure measurements with numerical simulations (§ 4.7), would translate in a wider eroded area and a reduced impact of the resolution of the sensor on the measured temperature anomaly.

5 Prediction of the thermal response of a dike to seepage flow and piping

5.1 Theoretical model

Heat transfer in porous media is described by the following form of the advection-diffusion equation:

$$\frac{\partial T}{\partial t} + \nabla \cdot \left(\frac{\rho_w c_w}{C} \mathbf{u} T \right) = \nabla \cdot \left(\frac{\lambda}{C} \nabla T \right) \qquad (1)$$

where T is the temperature, ρ_w and c_w are density and specific heat capacity of water, C is the volumetric heat capacity of the soil and λ the thermal conductivity of the soil. Typical values of the thermal properties are given in Table 1. The second term of the left-hand side is the advective term and describes the transport of heat operated by the fluid moving in the pores. **u** is the specific discharge rate, which is given by the Darcy's formula:

$$\mathbf{u} = -K \nabla \left(\frac{p}{\rho_w g} + z^* \right). \qquad (2)$$

In Eq. (2) K is the hydraulic conductivity, ρ_w is the density of water, p is the porewater pressure, z^* is the elevation and g is the gravitational constant. The quantity

$$\mathbf{v}_T = \frac{\rho_w c_w}{C} \mathbf{u} \qquad (3)$$

is usually referred to as the thermal front velocity. Although it is not the exact velocity at which a thermal front advances, since it neglects the effect of conduction, it is considered an accurate measure of the front velocity. The right-hand side contains the diffusive term that describes the effect of heat conduction. The quantity

Hydrol. Earth Syst. Sci. Discuss., doi:10.5194/hess-2016-662, 2017
Manuscript under review for journal Hydrol. Earth Syst. Sci.
Published: 9 January 2017

$$a = \frac{\lambda}{C} \qquad (4)$$

is called thermal diffusivity and is a measure of the inertia of the medium to temperature changes.

Eq. (1) neglects thermal dispersion, which takes into consideration the spreading of heat caused by the fluctuation of the micro-streamlines with respect to the main fluid flow direction because of the existence of a pore system. Although in solute transport - which is described by the same equations as heat transfer - dispersion is significant, Rau et al. (2012) describe how, at the sub-meter scale, dispersion of heat in soils is negligible. Dispersion can however occur at a larger scale because of the combined variability of micro-streamlines and hydraulic conductivity.

In the absence of water flow, the temperature in the shallowest portion of the subsoil (up to 10-15 m depth) fluctuates annually, mostly as a consequence of the variations in the air temperature and solar radiation, and can be estimated according to a model proposed by Hillel (1998). The model was derived solving Eq. (1) in a 1-d domain for **u** = 0. The model assumes that the temperature at the soil surface ($z = 0$) has a sinusoidal variation throughout the year:

$$T(t) = T_a + A_0 \sin\left[\omega(t - t_0) + \phi\right], \qquad (5)$$

where T_a is the mean soil temperature, A_0 is the amplitude of the annual temperature function, $\omega = 2\pi/365$ is the angular speed, t is the day of the year (starting counting from an arbitrary day), t_0 is the time lag between the occurrence of the minimum temperature in a year and the arbitrary reference day. If 1st January is considered as a reference, then the phase shift is $-\pi/2$ in the Northern Hemisphere. The model also assumes that at infinite depth the soil temperature is constant and equal to T_a. The temperature at any depth z is then a sine function of time and can be represented as:

$$T(z,t) = T_a + A_0\, e^{-z/d}\left[\sin\ \omega(t - t_0) - \frac{z}{d} + \phi\right]. \qquad (6)$$

The constant d is a characteristic depth, called damping depth, at which the temperature amplitude decreases to the fraction $1/e$ of the amplitude at the soil surface. It is related to the thermal diffusivity of the soil and the frequency of the temperature fluctuation:

$$d = (2a/\omega)^{1/2}. \qquad (7)$$

If the air temperature is used as input instead of the surface temperature, Nofziger (2005) suggests increasing it of 2 °C to take into account the effect of solar radiation. The correction is valid for bare soils, while it should be smaller for vegetated soils.

5.2 Propagation of an advective front: the geothermal Péclet number

As stated in Sec. 4, if a thermal front propagates from upstream up to the downstream toe during a flood event, the onset of piping causes the formation of thermal anomalies that can be exploited for early warning purposes. The propagation of the front, in turn, requires that advection prevails over the whole seepage length and that the time required by the thermal front to reach the downstream toe is much smaller that the duration of the flood event.

In transport problems, the relative importance of convection over conduction is described by the Péclet number. The latter is derived applying dimensional analysis to Eq. (1) written for a one-dimensional domain and its definition is:

Hydrol. Earth Syst. Sci. Discuss., doi:10.5194/hess-2016-662, 2017
Manuscript under review for journal Hydrol. Earth Syst. Sci.
Published: 9 January 2017

$$\mathrm{Pe} = \frac{u\, l\, C_\mathrm{w}}{\lambda}, \qquad (8)$$

where l is the characteristic length, that is a length representative of the phenomenon under investigation. Exact threshold values for the Péclet number do not exist, but for values much less than unity conduction is dominant, whereas for values significantly greater than unity advection prevails. For values in the order of 1 the behaviour of the system is intermediate.

Applying dimensional analysis to the closed hydrogeological system depicted in Fig. 12, where the conductive heat flow is mainly vertical and the fluid flow can be both horizontal and vertical, Van der Kamp and Bachu (1989) defined a parameter that gives an estimate of the relative magnitude of advective and conductive heat fluxes over a two-dimensional domain. They named it geothermal Péclet number and its definition is:

$$\mathrm{Pe_g} = \frac{q_\mathrm{H}\, C_\mathrm{w}\, D\, A}{\lambda}. \qquad (9)$$

In the formula, q_H is the horizontal specific discharge (or average horizontal Darcy velocity), D is the thickness of the hydrological system and $A = D/L$ is the aspect ratio of the representative element of the seepage domain, where L is given by the horizontal size of the flow path. Conduction in the horizontal direction is neglected. Van der Kamp (1984) pointed out that Eq. (9) represents the ratio of the amount of horizontally convected horizontally heat (approximately equal to $q_\mathrm{H} C_\mathrm{w} D \Delta T$, where ΔT is the change in temperature between the top and bottom of the system) to the amount of heat transferred vertically by conduction (approximately equal to $\lambda L \Delta T / D$).

The most common discussion around Péclet numbers is about the choice of the characteristic length. In hydrogeological systems the characteristic length is related to the vertical size of the domain but the choice of its value is not straightforward. Van der Kamp and Bachu (1989) leave the question open for hydraulically non-homogeneous systems, i.e. systems where the fluid flow is concentrated in a layer of limited thickness compared to the depth of the system.

As far as our problem is concerned, the position of the top boundary is well known because it coincides with the surface of the embankment, but the position of the lower boundary is undefined. In this work an approximation has been made: the top and lower bottom of the model are assumed to coincide with the top and bottom boundary of the layer where seepage occurs, as shown in Fig.13. With this assumption the geothermal Péclet number takes into account a conductive flux slightly larger than the actual one. Differently from the model in Fig. 12, it is assumed that the temperatures at the top and bottom boundary are equal and significantly different from the inflow temperature.

A parametric analysis with a finite element model (Bersan 2015) showed that the behaviour of such system can be predicted by Eq. (9) if D is substituted by $D/2$. Indeed, differently from the system in Fig. 12, where conduction occurs in a single direction, here conduction occurs from the centre of the domain both upwards and downwards. The parametric analysis showed that for values of the geothermal Péclet number lower than 1 the system is conduction-controlled, for values between 1 and 10 the behaviour is intermediate whereas for values larger than 10 the system is advection-controlled.

In Fig. 14 the geothermal Péclet number is plotted as a function of D, the thickness of the sand layer, and L, the distance along the seepage path. If the behaviour at the downstream toe is searched for, L must be chosen equal to the width of the dike at the base. Choosing smaller values, the behaviour at any other point along the seepage path is predicted. Two cases are

Hydrol. Earth Syst. Sci. Discuss., doi:10.5194/hess-2016-662, 2017
Manuscript under review for journal Hydrol. Earth Syst. Sci.
Published: 9 January 2017

plotted in Fig. 14: a very permeable sand layer ($K = 10^{-3}$ m/s) and a sand layer of medium permeability ($K = 10^{-4}$ m/s) both subject to a horizontal gradient of 0.1, which is a value large enough for triggering piping. The time required by the thermal front to reach the downstream toe, estimated using the thermal front velocity in Eq. (3), can be read on the top x-axis as a function of L. This estimate represents an upper bound, since the effect of conduction is neglected, but the approximation is reasonably good. For $K = 10^{-3}$ m/s, the expected behaviour is intermediate or advective for every possible size of the dike and a thickness of the sand layer larger than 1. The time required for the front to reach downstream is in the order of few days. For $K = 10^{-4}$ m/s the expected behaviour is purely conductive if the sand layer is thinner than 3-4 m. However, the main constraint for a riverdike seems to be the time required for the front to reach downstream, which is in the order of tens of days for a medium/large dike.

Considering the strong approximation made on the boundary conditions, numerical analysis is recommended for in-depth studies to verify the quality of the predictions made using the Péclet number. Transient analyses are to be preferred to steady state analyses to limit the influence that the position of the boundaries has on the solution, no matter of how far from the region of interest they are placed.

5.3 Alteration of the initial temperature gradient

5.3.1 Horizontal gradient under a dike

By geometry, the distance between the base and the surface of an embankment increases from the toes to the crest. Since an increasing distance from the surface translates in an increasing damping and phase shift in the propagation of the temperature wave in the soil, a temperature gradient is present at the base of a dike in the direction of the seepage flow. Fig. 15 shows the temperature at the base of a 1:2 slope as calculated using a finite element code. Eq. (5) was applied as boundary condition at the surface of the slope with the following parameters: $T_a = 9.0$ °C, $A_0 = 8.5$ °C, $t_0 = 20$ d. At depth, at the bottom boundary, a constant temperature value, equal to the annual average T_a, was assigned.

Since the amplitude of the annual temperature variation in the soil decreases exponentially with depth, the gradient along the base of an embankment slope is higher where the base is closer to the surface, i.e. at the toe, and very small where the base is far from the surface, i.e. near the crest. This appears clearly in Fig. 16 where the horizontal temperature gradient at the base of the embankment is plotted in absolute value. It can also be noted that the gradient is smaller during the mid seasons. Moreover, the sensitivity of the model to the soil thermal properties was tested and the results show that decreasing the thermal conductivity and heat capacity of the embankment soil (which means assuming higher clay content and/or lower degree of saturation) the gradient slightly increases in a region close to the toe. At very small depth (< 1 m), thus very close to the toe, daily temperature variations and solar radiation, that were not taken into account in the model, can contribute to increase or decrease - depending on the period of the year - the gradient.

The decrease of the gradient with increasing distance from the surface has also a drawback on piping detection that is worthwhile to investigate. In the experiment described in this paper the dike rested directly on a sand layer prone to piping,

Hydrol. Earth Syst. Sci. Discuss., doi:10.5194/hess-2016-662, 2017
Manuscript under review for journal Hydrol. Earth Syst. Sci.
Published: 9 January 2017

so that the interface where piping developed (and where temperature was monitored) was very shallow in the proximity of the toe. However, if the piping-prone layer is deeper, overlain by an impervious soil layer, the gradient along the seepage path could be not large enough to enable piping detection. In Fig. 17 the horizontal gradient is represented as a function of depth. Rather than the local gradient, the temperature difference between the dike toe and a point along the seepage path (x = 1, 3 and 5 m) is plotted. If it is assumed that a minimum temperature difference of 0.2 °C between the position of the sensor (in this case at the dike toe) and the head of a pipe (in this case 1, 3 or 5 m long) is necessary to guarantee piping detection, then some "shadow zones" (indicated in the figure by a grey shading) are delimited. These zones, where temperature measurements are likely to be ineffective at least in some periods of the year, occur beyond 1.25 m from the ground level. This means that if the interface between a top impervious layer and a sandy piping-prone layer is more than 1.25 m deep, the initial gradient could be too small to enable piping detection. The plots also show that the longer the pipe the smaller the shadow zones.

5.3.2 Vertical gradient under a dike

This condition is more complicated than that described in the previous section. Although most of the water enters in a pipe in proximity of the head, a pipe induces a modification of the seepage velocity field all along its length. As depicted in Fig. 18, the flow lines bend and at the bottom of the pipe the vertical component of the seepage flux becomes significant. Such component modifies the initial temperature gradient existing in the vertical direction. The thermal anomalies arising are therefore the superposition of: (1) the effect of the increased flow velocity in the pipe and in the area behind the head of the pipe; (2) the effect of the horizontal flow to the pipe in the direction perpendicular to the main seepage flow; (3) the effect of the vertical flow to the pipe. The importance of the latter lies in the fact that the alteration of the thermal vertical gradient can generate a thermal anomaly not only inside the pipe or in a very small region around it but also tens of centimetres under the pipe. Therefore a sensor could record a temperature anomaly even though not located exactly at the depth where the pipe develops. This is helpful because in existing dikes it is very difficult to deploy the sensor with centimetric accuracy at the depth where piping is expected to occur. In highly heterogeneous soils it can be even difficult to predict the exact depth where piping will occur.

6 Conclusions

The paper examines the effect of seepage and backward erosion piping on the temperature distribution under a dike. In particular, the effect of transient hydraulic loads, typical of river embankments, is analysed.

Data from a field trial conducted on a purpose-built dike suggest that seepage can affect the temperature distribution in different ways and that piping detection through the thermometric method requires the existence of a temperature gradient along the pipes.

Hydrol. Earth Syst. Sci. Discuss., doi:10.5194/hess-2016-662, 2017
Manuscript under review for journal Hydrol. Earth Syst. Sci.
Published: 9 January 2017

The first possible consequence of seepage under a dike is the propagation of a thermal front with temperature equal to the temperature of the waterbody. Since soils prone to backward erosion piping are rather permeable, seepage rates are often high enough to enable the transfer of heat by advection, which means that the water entering upstream of the dike reaches the landside maintaining its initial temperature. Two tools are suggested in this paper to ascertain, case by case, if a thermal front will propagate along the seepage path: the geothermal Péclet number and the thermal front velocity. The geothermal Péclet number predicts the importance of advection over conduction in hydrogeological systems. The thermal front velocity, which is proportional to the seepage rate, approximately informs about the distance that a thermal front travels along the seepage path during a flood event. If the advective front approaches the head of a pipe before the highest water level is reached in the river, than a gradient arises along the pipe enabling its early detection.

Because of the interaction between the soil and the atmosphere, the temperature at the base of dike is not uniform. A temperature gradient is always present, with the temperature at the toes being more similar to the actual air temperature and the temperature under the crest being more similar to the annual mean of the air temperature. Given this non-uniform initial condition, the onset of seepage produces a continuous temperature variation under a dike. If advection prevails, as in the field trial, the temperatures vary both in the foundation soil and in the pipes, but at a faster rate in the latter. If conduction prevails the temperature varies only in the pipes, where the seepage rate is very high. A sensor located at the downstream toe of a dike can record these temperature variations immediately after seepage begins; detection of piping is thus enabled since the very beginning of the flood event. Numerical simulations suggest that when the permeable layer is located at a depth larger than 1 m from the ground level the initial gradient might be not large enough to enable piping detection in some seasons.

In conclusion, some indications are given to predict the effect of backward erosion piping on the temperature distribution in order to optimize the design of early warning systems. Considering the approximations made and the large number of variables at stake, future research involving numerical modelling of the temperature variations induced by piping and in-depth analysis of additional field data would be beneficial for the validation of the ideas developed in this work.

Acknowlwdgements. We are thankful to the Fondazione Cassa di Risparmio di Padova e Rovigo that founded the project Riversafe, on the use of fiber optic sensors for levee monitoring. The analysis of the field data was performed within the project.

References

Aman, A. A. and Bman, B. B.: The test article, J. Sci. Res., 12, 135–147, doi:10.1234/56789, 2015.

Aman, A. A., Cman, C., and Bman, B. B.: More test articles, J. Adv. Res., 35, 13–28, doi:10.2345/67890, 2014.

Hydrol. Earth Syst. Sci. Discuss., doi:10.5194/hess-2016-662, 2017
Manuscript under review for journal Hydrol. Earth Syst. Sci.
Published: 9 January 2017

Allan, R. J., Douglas, K., and Peirson, W. L.: Development of an experimental research program into backward erosion piping, in: Proceedings of the 7th International Conference on Scour and Erosion, Perth, Australia, 2-4 December 2014, 249-255, 2014.

Artiéres, O., Bonelli, S., Fabre, J.-P., Guidoux, C., Radzicki, K., Royet, P., and Vedrenne, C.: Active and passive defences against internal erosion of dikes, in: Assessment of the risk of internal erosion of water retaining structures: dams, dikes and levees. Intermediate report of the working group of ICOLD, Deutsches Talsperren Komitee, Technical University of Munich, 114, 2007.

Bersan, S.: Piping detection in dike foundations by distributed temperature sensing: Understanding the development of thermal anomalies, Ph.D. Thesis, University of Padova, Italy, 2015.

Bligh, W. G.: Dams, barrages and weirs on porous foundations, Engineering News, 64(26), 708-710, 1910.

van Beek, V. M., Knoeff, H., and Sellmeijer, H.: Observations on the process of backward erosion piping in small-, medium- and full-scale experiments, European Journal of Environmental and Civil Engineering, 15(8), 1115-1137, 2011.

van Beek, V. M., Bezuijen, A., Sellmeijer, J. B., and Barends, F. B. J.: Initiation of backward erosion piping in uniform sands, Géotechnique, 64(12), 927-941, 2014a.

van Beek, V. M., Vandenboer, K., van Essen, H. M., and Bezuijen, A.: Investigation of the backward erosion mechanism in small scale experiments, in: Proc. of the 8th International Conference on Physical Modelling in Geotechnics, Perth, Australia, 14-17 Jan. 2014, 855-861, 2014b.

Clibborn, J., and Beresford, J.S.: Experiment on passage of water through sand, Government of India, Central Printing Office, 1902.

Henault, J.-M., Moreau, G., Blairon, S. et al.: Truly distributed optical fiber sensors for structural health monitoring: From the telecommunication optical fiber drawling tower to water leakage detection in dikes and concrete structure strain monitoring, Advances in Civil Engineering, 2010, Article ID 930796, 2010.

Hillel, D: Environmental soil physics, Academic Press, San Diego, CA, 1998.

ICOLD (International Commission on Large Dams) (Eds.): Internal erosion of existing dams, levees and dikes, and their foundations, Bullettin 164, vol. 1, Paris, France, 2015.

Imre E., Nagy, L., Lörincz, J., Rahemi, N., Schanz, T., Singh, V. P., Fityus, S., Some comments on the entropy-based criteria for piping, 17(4), 2281-2303, 2015.

Johansson, S., and Hellström, G.: DamTemp: Software package for evaluation of temperature field in embankment dams, HydroResearch and NeoEnergy, http://www.hydroresearch.se/en/temperature/evaluation, 2001.

Johansson, S., and Sjödal, P.: A guide for seepage monitoring of embankment dams using temperature measurements. CEATI Report No. T062700-0214, CEATI International Inc., Dam Safety Interest Group, Montreal, Quebec, Canada, 2009.

van der Kamp, G.: Evaluating the influence of groundwater flow systems on geothermal conditions, in: Energy Developments: New Forms, Renewable, Conservation, ed. F.A. Curtis, Pergamon Press, 297–301, 1984.

van der Kamp, G., and Bachu, S.: Use of dimensional analysis in the study of thermal effects of various hydrogeological regimes, in: Hydrogeological Regimes and Their Subsurface Thermal Effect, Geophysical Monograph Series, 47, ed. A.E. Beck, G. Garven, and L. Stegena, American Geophysical Union, Washington, DC, 23–28, 1989.

Kanning, W.: The weakest link. Spatial variability in the piping failure mechanism of dikes, Ph.D. thesis, Delft University of Technology, Delft, the Netherlands, 2012.

Khan, A. A., Vrabie, V., Mars, J. I., Girard, A., and d'Urso, G.: A source separation technique for processing of thermometric data from fiber-optic DTS measurements for water leakage identification in dikes, Sensors Journal, 8(7), 1118-1129, 2008.

Koelewijn, A. R., De Vries, G., Van Lottum, H., Förster, U., van Beek, V. M., and Bezuijen, A.: Full-scale testing of piping prevention measures: Three tests at the IJkdijk, in: Proc. of the 8th International Conference on Physical Modelling in Geotechnics, Perth, Australia, 14-17 Jan. 2014, 891-897, 2014.

Koelewijn, A. R., and Taccari, M. L.: LiveDijk Willemspolder, Praktijkproeven Verticaal Zanddicht Geotextiel en grofzandbarrière [Live dike Willemspolder, tests in practice on a geotextile barrier and a coarse sand filter against piping], report no. 1208555-000-GEO-0006, Deltares, Delft, 2016.

Müller-Kirchenbauer, H., Rankl, M., and Schötzer, C.: Mechanism for regressive erosion beneath dams and barrages, Filters in Geotechnical and Hydraulic Engineering, J. Brauns, M. Heibaum, and U. Schuler eds., Balkema, Rotterdam, the Netherlands, 369-376, 1993.

Ng, G., and Oswalt, K.: Levee monitoring system. Better management through better information, Engineering Systems, April 2010, 1-12, 2010.

Nofziger, D. L.: Soil temperature changes with time and depth: Theory, http://soilphysics.okstate.edu/software/SoilTemperature/document.pdf, 2005.

Ojha, C. S., and Singh, V. P.: Determination of critical head in soil piping, Journal of Hydraulic Engineering, 129(1), 511-518, 2003.

Peeters, P., Haelterman, K., and Visser, K. P.: About reinventing innovative technologies for levee monitoring, ICOLD 2013 International Symposium, Seattle, WA, 2013.

Rau, G. C., Andersen, M. S., and Acworth, R. I.: Experimental investigation of the thermal dispersivity term and its significance in the heat transport equation for flow in sediments, Water Resour. Res., 48(3), W03511, 2012.

Richards, K. S. and Reddy, K. R.: True triaxial piping test apparatus for evaluation of piping potential in earth structures, Geotechnical Testing Journal, 33(1), 2014.

Schmertmann, J. H.: The non-filter factor of safety against piping through sands, in: Judgment and Innovation, Geotechnical Special Publication No. 111, F. Silva and E. Kavazanjian eds., ASCE, Reston, VA, 65-132, 2000.

Sellmeijer, H., de la Cruz, J. L., van Beek, V. M., and Knoe, H.: Fine-tuning of the backward erosion piping model through small-scale, medium-scale and IJkdijk experiments, European Journal of Environmental and Civil Engineering, 15(8), 1139-1154, 2011.

Hydrol. Earth Syst. Sci. Discuss., doi:10.5194/hess-2016-662, 2017
Manuscript under review for journal Hydrol. Earth Syst. Sci.
Published: 9 January 2017

Sheffer, M. R., Johansson, S., and Sjödahl, P.: Recent developments in the use of temperature, resistivity and self-potential methods for monitoring embankment dam performance, Annual Conference Canadian Dam Association, 3-8 October 2009, Whistler, BC, Canada, 2009.

TAW (Technische Adviescommissie voor de Waterkeringen): Technisch rapport zandmeevoerende wellen [Technical report on sandboils], Rijkswaterstaat, the Netherlands, 1999.

Terzaghi, K.: Der grundbruch an stauwerken und seine verhüting [The failure of dams by piping and its prevention], Die Wasserkraft, 17(24), 445-449, 1922. Reprinted in: Terzaghi, K.: From theory to practice in soil mechanics, Wiley, New York, NY, 114-118, 1960.

USACE (U.S. Army Corps of Engineers): Design guidance for levee underseepage, Technical letter no. 1110-2-569, Washington, DC, 2005.

Wang, D. Y., Fu, X. D., Jie, Y. X., and Feng, Q. F.: How a suspended cut-off wall functions: Effect of soil anisotropy in a levee foundation, in: Proceedings of the 7th International Conference on Scour and Erosion, Perth, Australia, 2-4 December 2014, 129-136, 2014.

Weijers, J. B. A., and Sellmeijer, J. B.: A new model to deal with the piping mechanism, Filters in geotechnical and hydraulic engineering, J. Brauns, U. Schuler, and M. Heibaum, eds., Balkema, Rotterdam, the Netherlands, 349-355, 1993.

WES (U.S. Army Corps of Engineers Waterways Experiment Station): Investigation of underseepage and its control: Lower Mississippi river levees, Technical memorandum no. TM-3-424, Vicksburg, MS, 1956.

de Wit, J. M., Sellmeijer, J. B., and Penning, A.: Laboratory testing on piping, in: Proceedings of the 10th International Conference on Soil Mechanics and Foundation Engineering, 15-19 June 1981, Stockholm, Sweden, 517-520, 1981.

Hydrol. Earth Syst. Sci. Discuss., doi:10.5194/hess-2016-662, 2017
Manuscript under review for journal Hydrol. Earth Syst. Sci.
Published: 9 January 2017

Hydrology and Earth System Sciences
Open Access
Discussions

Table 1: Typical values of soil thermal properties.

Parameter	Value	Unit
Thermal conductivity of saturated sand	2.8	W m^{-1} K^{-1}
Thermal conductivity of saturated clay	1.4	W m^{-1} K^{-1}
Thermal conductivity of dry clayey	0.5	W m^{-1} K^{-1}
Specific heat capacity of water	4186	J kg^{-1} K^{-1}
Volumetric heat capacity of sat. sand	$2.8 \cdot 10^6$	J m^{-3} K^{-1}
Volumetric heat capacity of sat. clay	$2.5 \cdot 10^6$	J m^{-3} K^{-1}
Volumetric heat capacity of dry clay	$1.6 \cdot 10^6$	J m^{-3} K^{-1}

Hydrol. Earth Syst. Sci. Discuss., doi:10.5194/hess-2016-662, 2017
Manuscript under review for journal Hydrol. Earth Syst. Sci.
Published: 9 January 2017

Hydrology and Earth System Sciences
Discussions
Open Access
EGU

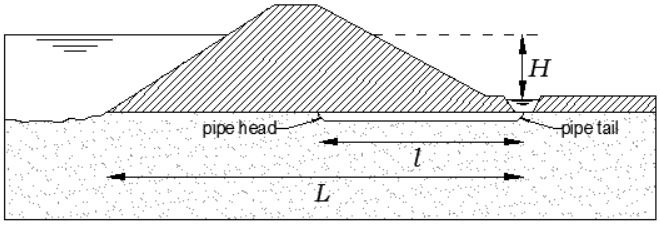

Figure 1: Backward erosion piping under a dike (adapted from ICOLD, 2015).

Figure 2: Large-scale piping facility

Hydrol. Earth Syst. Sci. Discuss., doi:10.5194/hess-2016-662, 2017
Manuscript under review for journal Hydrol. Earth Syst. Sci.
Published: 9 January 2017

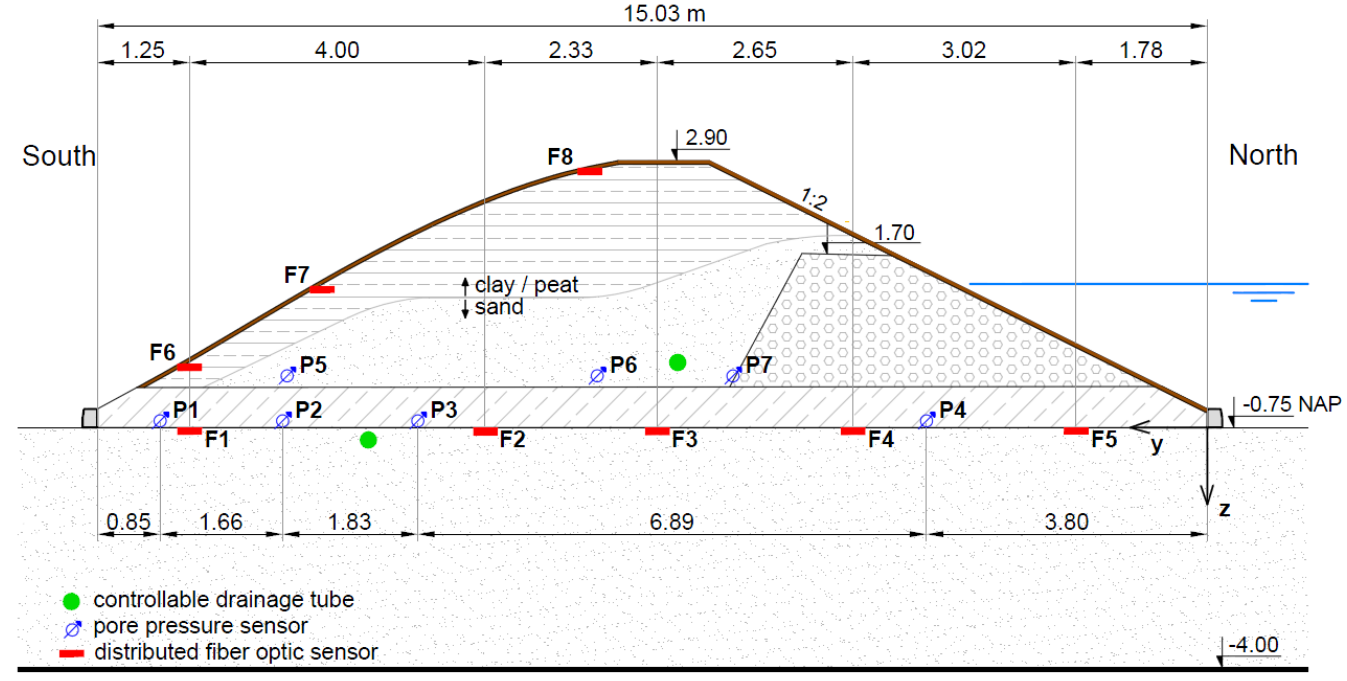

Figure 3: Cross section of the test dike with indicated the position of the sensors.

Figure 4: Geotextile strip encasing two single-mode and two multi-mode optical fibres.

Hydrol. Earth Syst. Sci. Discuss., doi:10.5194/hess-2016-662, 2017
Manuscript under review for journal Hydrol. Earth Syst. Sci.
Published: 9 January 2017

Hydrology and Earth System Sciences
Discussions

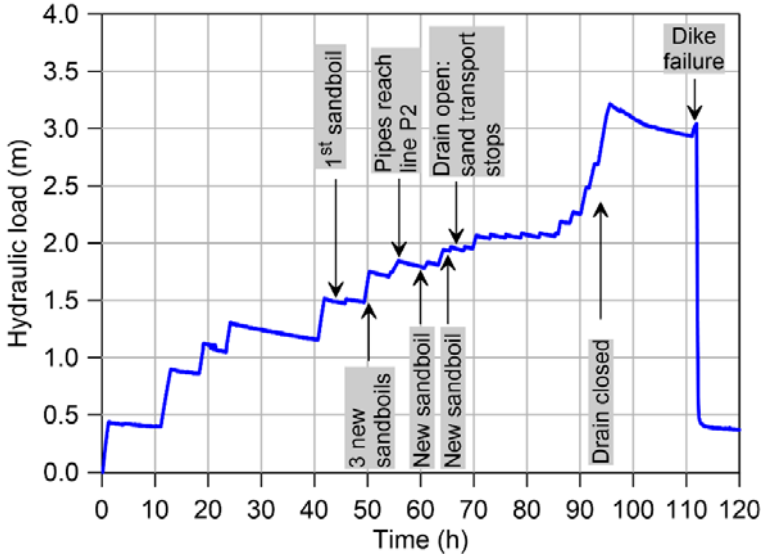

Figure 5: Hydraulic load applied to the test dike.

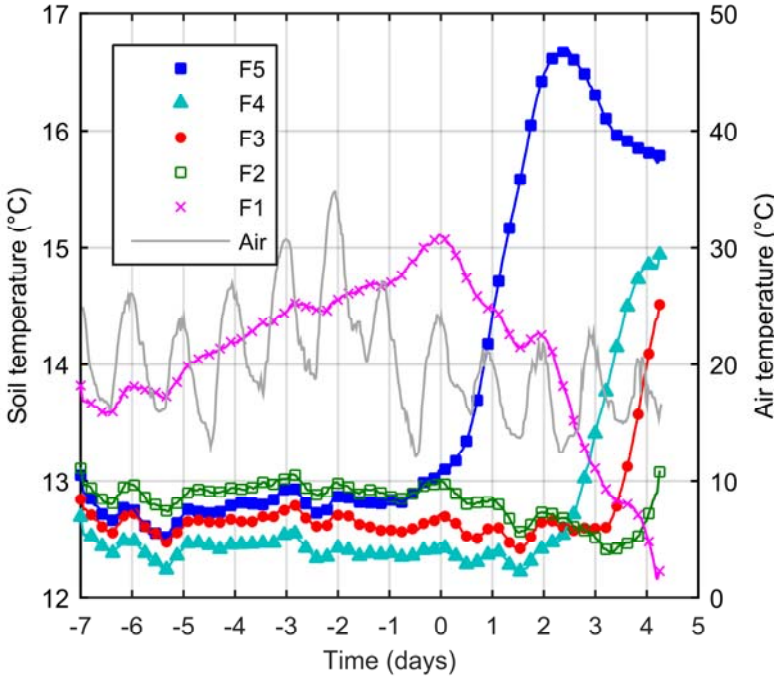

Figure 6: Temperature measured by the distributed temperature sensor at different distances from upstream (F1 to F5) at x=10 m.

Hydrol. Earth Syst. Sci. Discuss., doi:10.5194/hess-2016-662, 2017
Manuscript under review for journal Hydrol. Earth Syst. Sci.
Published: 9 January 2017

Hydrology and Earth System Sciences
Discussions
Open Access
EGU

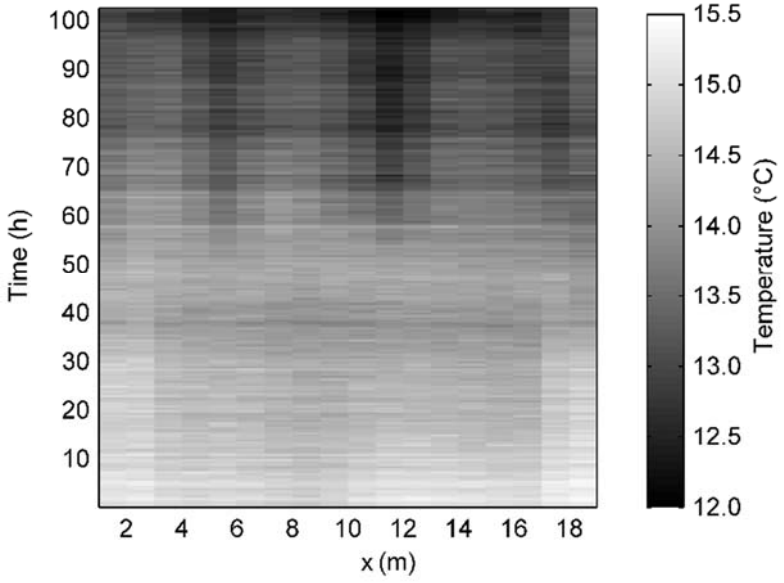

Figure 7: Temperature measured along the dike near the downstream toe (F1).

Hydrol. Earth Syst. Sci. Discuss., doi:10.5194/hess-2016-662, 2017
Manuscript under review for journal Hydrol. Earth Syst. Sci.
Published: 9 January 2017

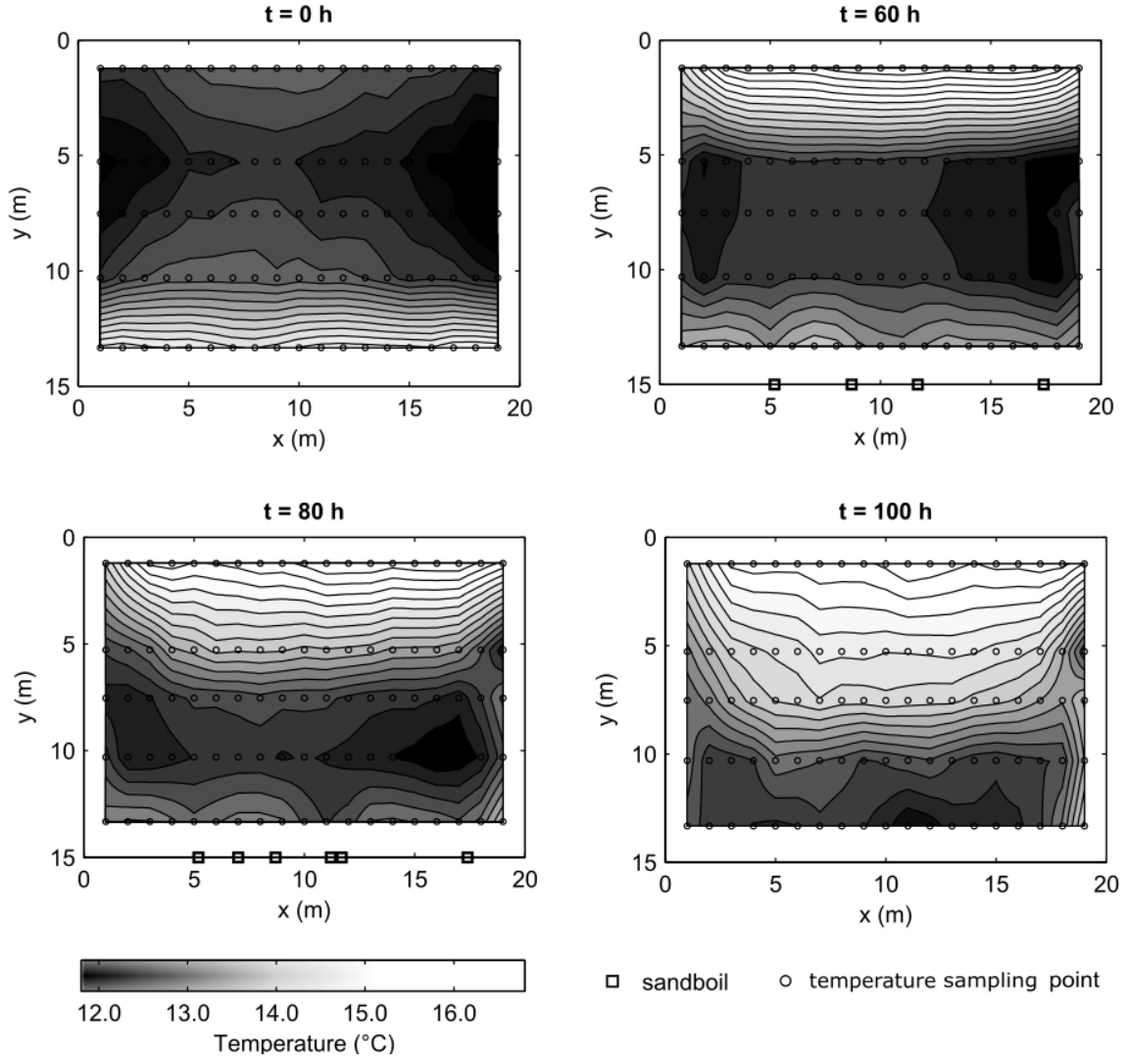

Figure 8: Temperature at the bottom of the dike at 0, 60, 80 and 100 h from the beginning of the test.

Hydrol. Earth Syst. Sci. Discuss., doi:10.5194/hess-2016-662, 2017
Manuscript under review for journal Hydrol. Earth Syst. Sci.
Published: 9 January 2017

Hydrology and Earth System Sciences
Discussions

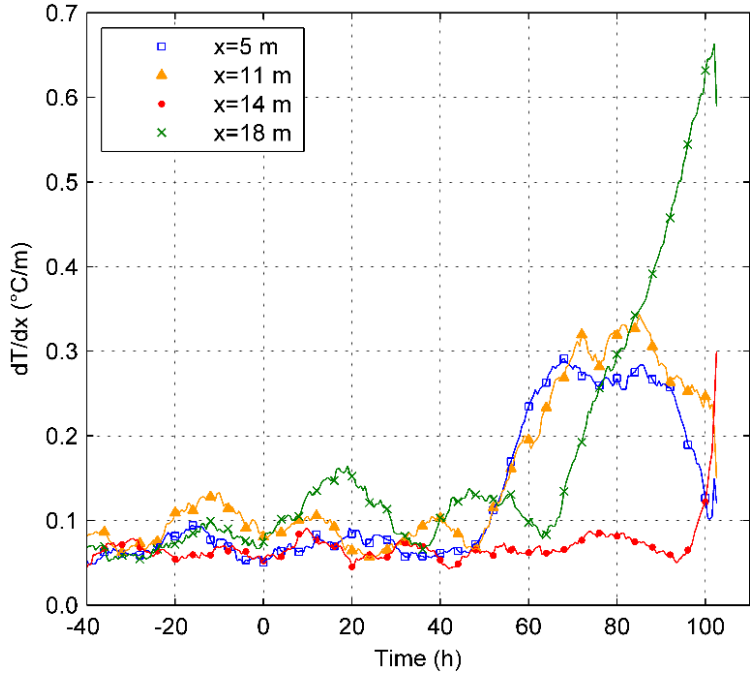

Figure 9: Temperature gradients along the most downstream line F1 at some significant points: at x=5 m, x=11 m and x=18 m sand-boils were observed; at x=18 m also likely preferential seepage path at the contact with the foil; at x=14 m: no traces of piping (until 90 h when visual inspection was suspended).

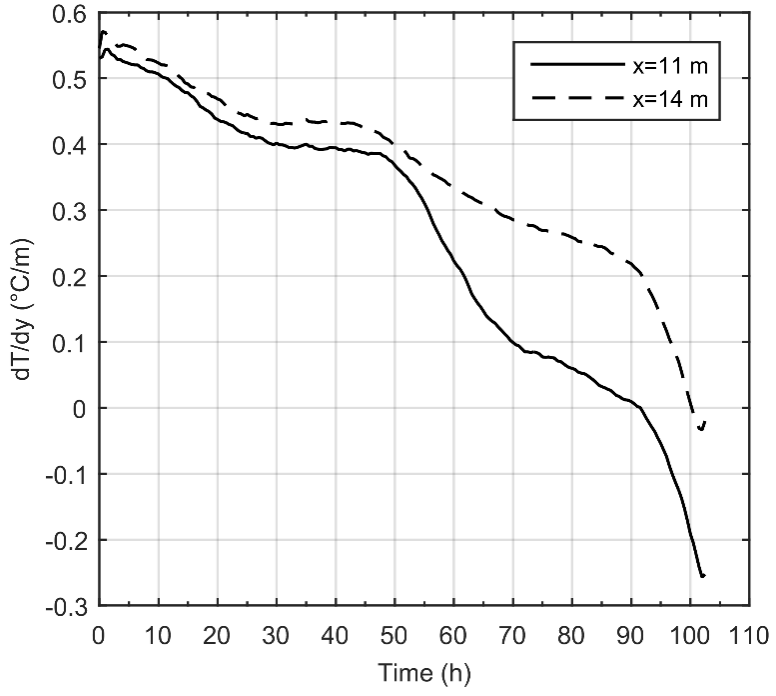

Figure 10: Temperature gradients in the direction of the seepage flow at a location affected by piping (x=11 m) and at a location where no piping was detected (x=14 m).

Hydrol. Earth Syst. Sci. Discuss., doi:10.5194/hess-2016-662, 2017
Manuscript under review for journal Hydrol. Earth Syst. Sci.
Published: 9 January 2017

Hydrology and Earth System Sciences
Discussions

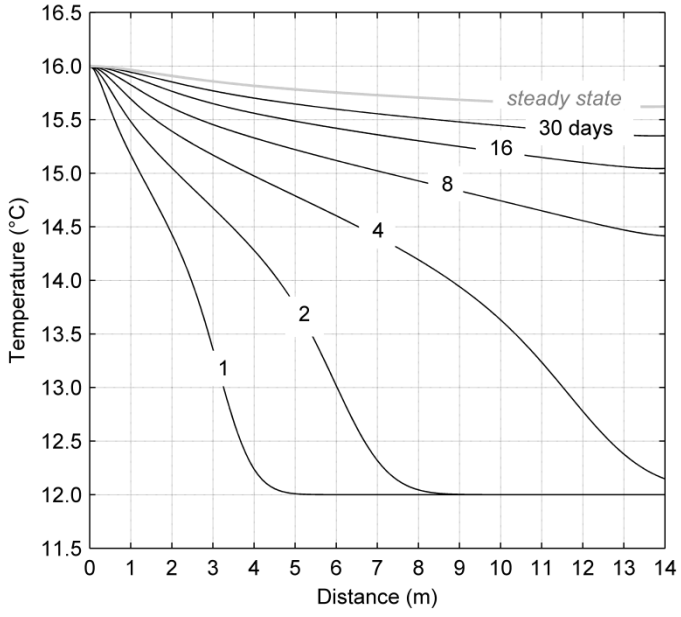

Figure 11: FE simulation of a thermal front propagating in the foundation of the test dike for a constant hydraulic load of 3 m and uniform initial temperature T=12 °C. On the x-axis the distance from the inflow point is indicated.

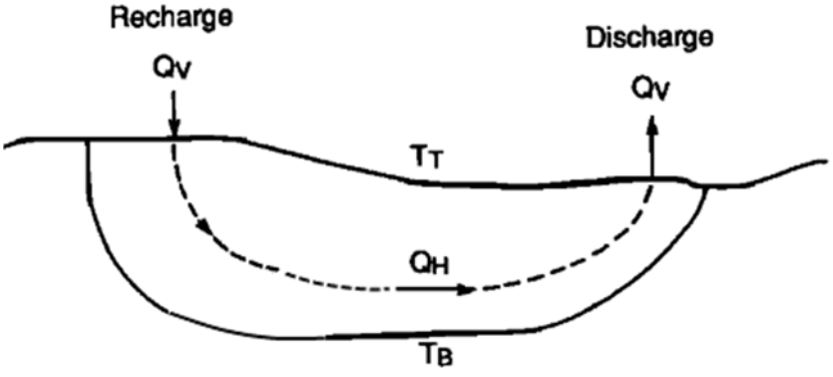

Figure 12: Open hydrogeological system (Van der Kamp and Bachu, 1989).

Hydrol. Earth Syst. Sci. Discuss., doi:10.5194/hess-2016-662, 2017
Manuscript under review for journal Hydrol. Earth Syst. Sci.
Published: 9 January 2017

Hydrology and Earth System Sciences
Discussions

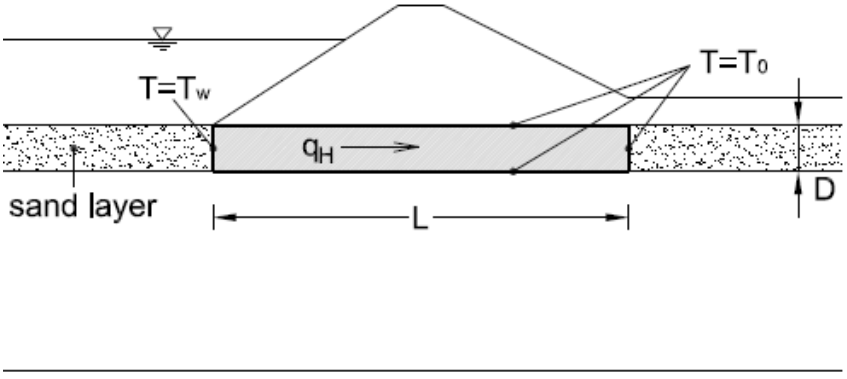

Figure 13: Domain (grey rectangle) and boundary conditions assumed for the calculation of the geothermal Péclet number.

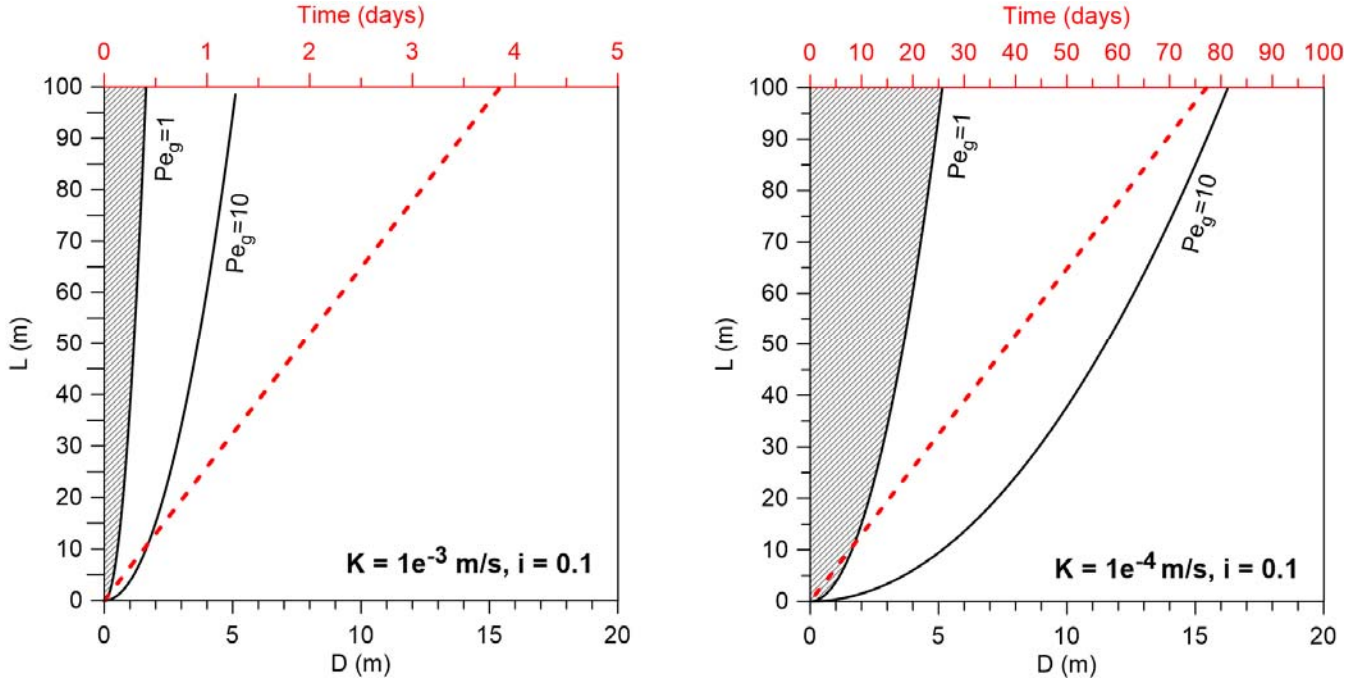

Figure 14: Threshold values of the geothermal Péclet number as a function of distance along the seepage path (L) and thickness of the sand layer (D) for two different permeability values (K) and average hydraulic gradient of 0.1. The dotted line indicates the arrival times of the thermal front, that must be read on the top x-axis as a function of distance L.

Hydrol. Earth Syst. Sci. Discuss., doi:10.5194/hess-2016-662, 2017
Manuscript under review for journal Hydrol. Earth Syst. Sci.
Published: 9 January 2017

Hydrology and Earth System Sciences
Discussions

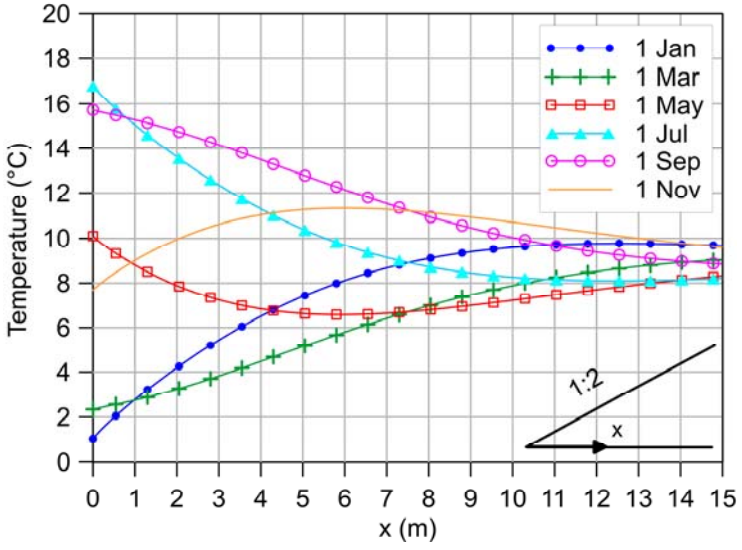

Figure 15: Temperature at the base of 1:2 slope from finite element modelling.

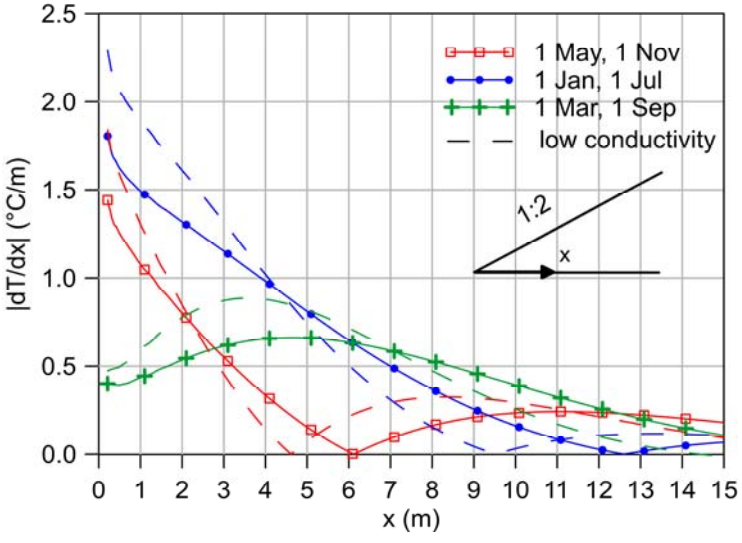

Figure 16: Horizontal temperature gradient at the base of 1:2 slope. Finite element solutions for average and low (dashed lines) thermal conductivity of the embankment soil.

Hydrol. Earth Syst. Sci. Discuss., doi:10.5194/hess-2016-662, 2017
Manuscript under review for journal Hydrol. Earth Syst. Sci.
Published: 9 January 2017

Hydrology and Earth System Sciences
Discussions

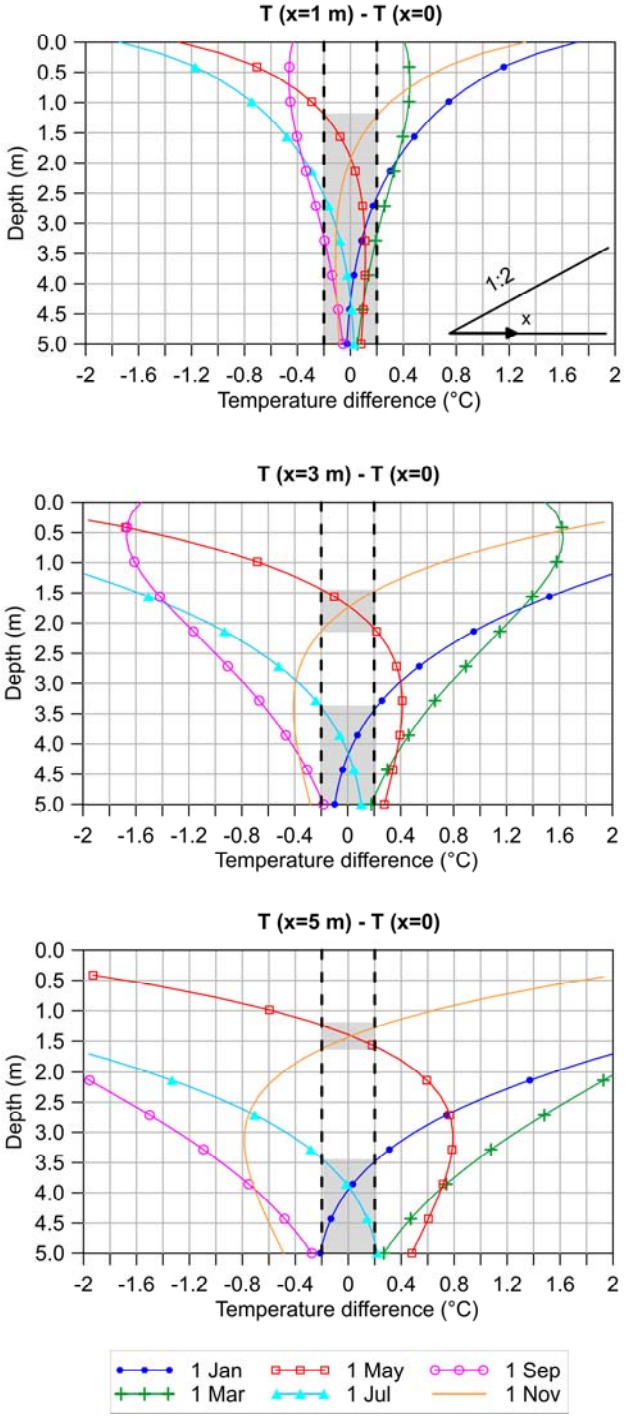

Figure 17: Temperature difference between the dike toe and a point along the seepage path (x = 1, 3 and 5 m) as a function of depth and period of the year. The regions where the temperature difference is smaller than 0.2 °C (in absolute value) are highlighted by a grey shading.

Hydrol. Earth Syst. Sci. Discuss., doi:10.5194/hess-2016-662, 2017
Manuscript under review for journal Hydrol. Earth Syst. Sci.
Published: 9 January 2017

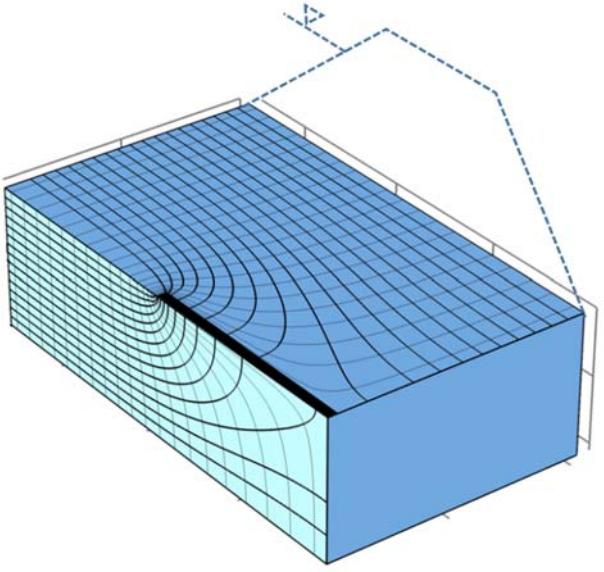

Figure 18: Flow net around a pipe (black rectangle) extending for half of the seepage length. Exploiting symmetry, only half of the problem is modelled.